ISSN 1063-7834, Physics of the Solid State, 2013, Vol. 55, No. 11, pp. 2205–2214. © Pleiades Publishing, Ltd., 2013.
Original Russian Text © E.V. Shalaeva, Yu.V. Chernyshev, E.O. Smirnova, S.V. Smirnov, 2013, published in Fizika Tverdogo Tela, 2013, Vol. 55, No. 11, pp. 2095–2104.

METALS

# Lamellar Structure and Nanomechanical Properties of Quasicrystalline Al–Cu–Fe Alloys

**E. V. Shalaeva[a, b, *], Yu. V. Chernyshev[a], E. O. Smirnova[c], and S. V. Smirnov[c]**

[a] *Institute of Solid State Chemistry, Ural Branch of the Russian Academy of Sciences, ul. Pervomaiskaya 91, Yekaterinburg, 620990 Russia*

** e-mail: shalaeva@ihim.uran.ru*

[b] *Ural Federal University named after the First President of Russia B. N. Yeltsin, ul. Mira 19, Yekaterinburg, 620002 Russia*

[c] *Institute of Engineering Science, Ural Branch of the Russian Academy of Sciences, ul. Komsomol'skaya 34, Yekaterinburg, 620219 Russia*

Received May 14, 2013

**Abstract**—The kinetics of structural phase transformations in quasicrystal-forming Al–Cu–Fe alloys with compositions in the region of stability of the icosahedral (*i*) phase has been investigated. It has been shown that, depending on the development of metastable transformations $i \longrightarrow$ pentagonal phases *P*1 and *P*2, a homogeneous lamellar structure ($i + P1 + P2$) or a polygrain *i*-phase is formed in the alloys. The *P*–*h* diagrams obtained upon nanoindentation, atomic force microscopy, and scanning electron microscopy of indentations have demonstrated signs of elasto-plastic deformation of the alloys with lamellar and polygrain icosahedral structures. It has been found that, in contrast to the polygrain icosahedral alloys with a normal size effect of nanoindentation, the alloys with a lamellar structure are characterized by a nonmonotonic dependence of the hardness (*H*) on the maximum load ($P_{max}$) and exhibit the effect of strain hardening in the range of loads 50 mN $\le P_{max} <$ 500 mN. The strain hardening is considered as the result of resistance exerted by boundaries of the lamellar structure to the development of plastic deformation.

**DOI:** 10.1134/S106378341311022X

## 1. INTRODUCTION

Since the discovery of aperiodic quasicrystalline phases in metal alloys, a great deal of attention has been paid to the investigation of their mechanical properties [1, 2]. Three-dimensional aperiodic icosahedral aluminum–transition metal quasicrystals, including those in the Al–Cu–Fe system, are characterized by high values of elastic moduli [3] and microhardness [4]. These properties provide the basis for their use as dispersion-strengthening phases and wear-resistant materials [5, 6]. The aforementioned practical applications require investigation of the mechanical properties of these materials not only in the bulk state but also under micro- and nanocontact loading using the indentation method. It has been found that there are significant differences in the mechanical properties of quasicrystals subjected to micro- or nanoindentation and macroscopic tests [6–9]. At room temperature, as was shown by tension and compression tests, quasicrystals are brittle materials. These phases exhibit plastic properties at high temperatures due to thermally activated processes of nucleation and motion of dislocations [1, 2]. In the case of micro- and nanoindentation, single-grain and polygrain aluminum–transition metal quasicrystals at low temperatures demonstrate signs of severe plastic deformation [6–10]. Among the problems that require a more detailed examination is the problem associated with the influence of the initial structural state of a quasicrystalline alloy on the plastic properties under nanocontact loading.

It is known that, in crystalline alloys, microstructural states, such as lamellar and polygrain icosahedral structures, can substantially affect the mechanical properties. It can be assumed that similar mechanisms will work for quasicrystalline alloys. Earlier, the hardening effect of quasicrystalline Al–Cu–Fe coatings with submicron-sized grains was demonstrated by Milman et al. [11] using a set of micro- and nanoindentation techniques. The formation of lamellar structures, as a rule, is the result of structural phase transformations associated either with doping the materials or with using their heat treatment. From this point of view, the Al–Cu–Fe system is of particular interest. In a narrow concentration range, which borders the region of stability, the icosahedral (*i*) phase of the Al–Cu–Fe system undergoes a series of structural transformations into the pentagonal approximant phases *P*1 and *P*2 [12, 13]. These transformations occur both in the equilibrium state and in rapidly quenched alloys. As compared to the icosahedral structure, the *P*1- and *P*2-phases lose their aperiodicity in one direction and can precipitate in the form of planar intergrowths that are coherently coupled with

the icosahedral matrix. It has also been found that, in quenched quasicrystal-forming Al–Cu–Fe alloys with compositions lying in the region of stability of the *i*-phase, the stage of formation of the perfect icosahedral structure is accompanied by the formation of planar defects in the form of intergrowths of the *P*1-structures [14].

The most interesting from the point of view of practical applications are alloys with compositions in the region of stability of the icosahedral phase, as well as the modification of their mechanical properties as a result of the formation of a homogeneous lamellar structure with planar intergrowths of pentagonal approximants.

In this work, the kinetics of transformations "icosahedral (*i*) quasicrystal ⟶ pentagonal phases" in the quasicrystal-forming $Al_{62.2}Cu_{24.8}Fe_{13}$ and $Al_{61.7}Cu_{25.2}Fe_{13.1}$ alloys with compositions in the region of stability of the *i*-phase has been investigated using transmission electron microscopy and electron diffraction, as well as the projection and cut method in the six-dimensional space. The possibility of forming a homogeneous lamellar structure of pentagonal phases has been demonstrated. The dependences of the loading curves and nanomechanical characteristics on the maximum load (in the range of 5–500 mN) have been examined using the nanoindentation method for two types of quasicrystalline alloys: (i) alloys with the lamellar structure of pentagonal phases and (ii) alloys with the single-phase polygrain icosahedral structure. It has been found that the quasicrystalline Al–Cu–Fe alloys with the lamellar structure exhibit a hardening effect.

## 2. METHODICAL PART

### *2.1. Techniques of the Preparation and Investigation of the Alloys*

Details of the preparation of quenched quasicrystal-forming alloys are described in our recent paper [14]. Isothermal annealings were performed in a helium atmosphere at temperatures of 550 and 650°C. The annealing times were 4, 8, 10, and 24 h. The local chemical analysis was carried out using the electron probe microanalysis method on a Cameca SX 100 microanalyzer at an accelerating voltage of 15 keV and a current of 29 nA. The standard deviations in the determination of the contents of the components Al, Fe, and Cu were equal to 0.14, 0.09, and 0.15 at %, respectively.

The structural investigations were carried out using transmission electron microscopy (JEM 200-CX microscope). For the electron microscopic examination, the obtained scales of the quenched alloy were electrolytically polished in a standard (methanol + nitric acid) mixture after the preliminary mechanical thinning.

The nanomechanical characteristics were investigated on test alloys with electrolytically polished surfaces. The *P–h* loading diagrams were obtained by measuring the indentation force (*P*) and the indentation depth (*h*) during indentation tests. In the range of loads from 5 to 50 mN, the measurements were performed on a TI900 Triboindenter automated nanomechanical test system equipped with an atomic force microscope. In the range of loads from 50 to 500 mN, the microhardness was measured on a FISCHERSCOPE HM2000 computer-controlled measuring system. The measurements in the TI900 Triboindenter system were carried out using a Berkovich indenter with the radius of curvature of 100 nm. In the FISCHERSCOPE HM2000, the measurements were made using a Vickers indenter.

The measuring systems were equipped with a special program for processing the *P–h* loading curves according to the Oliver–Pharr method, which made it possible to estimate the hardness from the parameters of the unloading branch of the *P–h* diagram and to take into account the correction for elastic recovery of indentation sizes and the deviation of the indenter tip from the ideal shape [15, 16]. The hardness (*H*) is determined as the averaged pressure in the contact (Meyer hardness) and can be calculated from the formula

$$H = P_{\max}/A(h_c), \tag{1}$$

where $P_{\max}$ is the maximum load; $A(h_c)$ is the projected area of the contact between the indenter and the material for the contact depth $h_c$,

$$h_c = h_{\max} - \eta P_{\max}/S; \tag{2}$$

$h_{\max}$ is the depth of contact at the maximum load $P_{\max}$; $S = dP/dh$ is the stiffness in contact; and $\eta$ is the geometrical factor, which takes into account the type of indenter. The projected contact area is estimated from the formula

$$A = C_0h_c^2 + C_1h_c + C_2h_c^{1/2} + C_3h_c^{1/4} + C_4h_c^{1/8} + C_5h_c^{1/16}, \tag{3}$$

where $C_0$, $C_1$, $C_2$, $C_3$, $C_4$, and $C_5$ are coefficients that are determined for the reference sample (fused silica). For Berkovich and Vickers indenters with ideal shapes, the contact areas are identical and defined by the formula $A = 24.5h_c^2$. The FISCHERSCOPE HM2000 system can also be used to determine the plastic hardness ($H_{Pl}$), which is calculated for the residual depth of the contact ($h_f$). The instrumental accuracy in the determination of the indentation depth *h* is equal to 0.1 nm. The experimental values of *H*, $h_c$, *S*, and *A* were determined from a series of measurements of the loading diagrams (from four to seven) for several samples of each type of alloys and for each load.

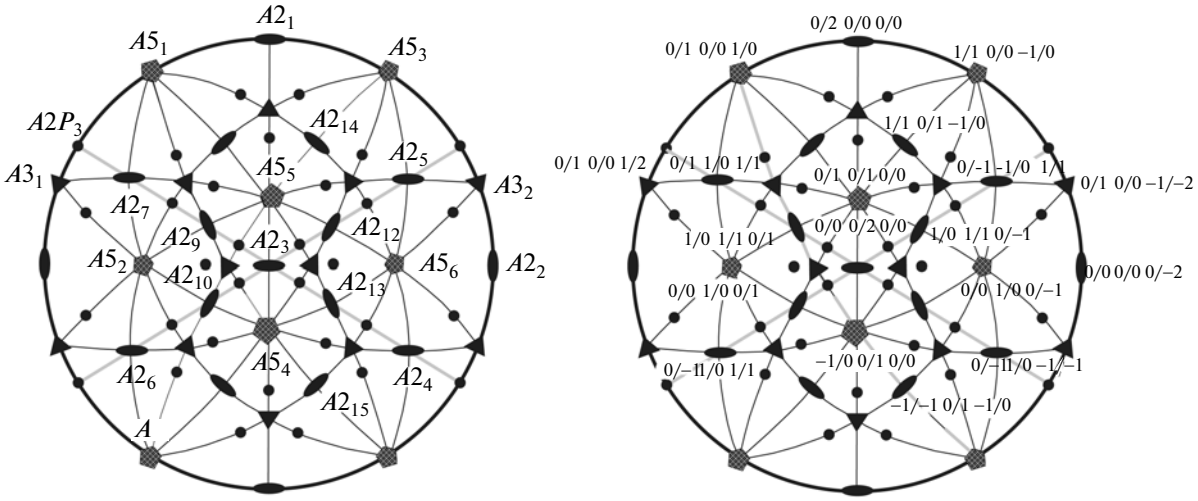


**Fig. 1.** Stereographic projection for the icosahedral space group ($m\overline{3}5$) in the direction of the twofold symmetry axis $A2_3$ [0/0 0/2 0/0]. The directions of the symmetry axes are indexed in the Cahn's six-index system [17].

### *2.2. Techniques of the Electron Diffraction and Electron Microscopic Analyses*

For the analysis of the electron diffraction patterns and the description of the reciprocal lattice of the icosahedral phase, we have used the projection and cut method in the six-dimensional space [17, 18]. According to this method, we can write

$$\mathbf{G} = \mathbf{g}_{\parallel} + \mathbf{g}_{\perp}, \tag{4}$$

where $\mathbf{G}$ is the vector of the periodic reciprocal lattice of the icosahedral phase in the six-dimensional space; and $\mathbf{g}_{\parallel}$ and $\mathbf{g}_{\perp}$ are the components of the reciprocal lattice vector in the three-dimensional parallel (physical space) and perpendicular spaces, respectively, defined by the six-dimensional projection matrix. The cross-sections of the reciprocal lattice of the icosahedral phase in the physical space were simulated in the three-dimensional cubic coordinate system with the $(3 \times 6)$ matrix. The $(3 \times 6)$ matrix transforms the six-dimensional reciprocal lattice vector $(n_1, n_2, n_3, n_4, n_5, n_6)$ of the $i$-phase, in which it is described by the periodic structure, into the three-dimensional physical aperiodic vector $(h + \tau h', k + \tau k', l + \tau l')$

$$g_{\parallel} = \begin{matrix} h + \tau h' \\ k + \tau k' \\ l + \tau l' \end{matrix} = \begin{pmatrix} 1 & \tau & 0 & -1 & \tau & 0 \\ \tau & 0 & 1 & \tau & 0 & -1 \\ 0 & 1 & \tau & 0 & -1 & \tau \end{pmatrix} \begin{pmatrix} n_1 \\ n_2 \\ n_3 \\ n_4 \\ n_5 \\ n_6 \end{pmatrix}, \tag{5}$$

where $\tau = \dfrac{(1+\sqrt{5})}{2}$. The simulation and indexing of the diffraction vectors $\mathbf{g}_{\parallel}(h/h', k/k', l/l')$ and directions in the electron diffraction patterns for the $i$-phase of the Al–Cu–Fe system (six-dimensional reciprocal lattice of the body-centered cubic (bcc) type) were performed in the primitive cell with superstructure reflections in the positions $(n_1 + 1/2, n_2 + 1/2, n_3 + 1/2, n_4 + 1/2, n_5 + 1/2, n_6 + 1/2)$, which was proposed in [19]. The stereographic projections for the orientation of the lattice of the $i$-phase ($m\overline{3}5$) used in the work are shown in Fig. 1.

## 3. EXPERIMENTAL RESULTS AND DISCUSSION

### *3.1. Formation of a Lamellar Structure of the Quasicrystal-Forming Al–Cu–Fe Alloys, Electron Diffraction and Electron Microscopy Investigations*

Figures 2 and 3 show the characteristic electron microscopy images and electron diffraction patterns of the quasicrystal-forming $Al_{62.2}Cu_{24.8}Fe_{13}$ and $Al_{61.7}Cu_{25.2}Fe_{13.1}$ alloys (with compositions in the region of stability of the $i$-phase) annealed at temperatures of 550 and 650°C for different times (4, 8, 10, 24 h).

The electron microscopy images of the quasicrystal-forming alloys (Fig. 2a) annealed at a temperature of 550°C for 4 or 8 h demonstrate a fringe contrast that is characteristic of planar defects in quasicrystalline structures with the displacement vector $\mathbf{R}$ at the boundary of the defect. These planar defects are located in all planes of the $i$-structure with fivefold symmetry axes. A typical diffraction pattern obtained from the region containing such defects and the corresponding calculated scheme are shown in Figs. 3a and 3b, respectively. In addition to the reflections of the $i$-phase, which are arranged according to the quasi-

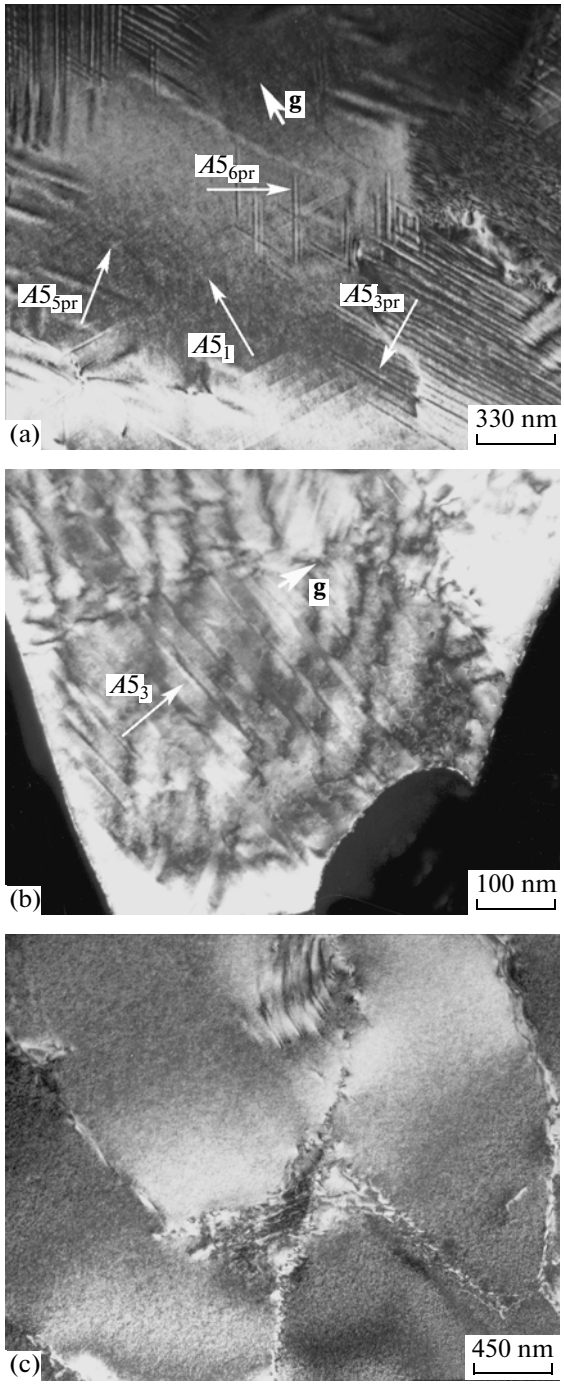


**Fig. 2.** Dark-field electron microscopy images of the quasicrystal-forming $Al_{62.2}Cu_{24.8}Fe_{13}$ alloy: (a) planar intergrowths of the $P1$-phase along the planes with the symmetry axes $A5$ for the orientation of the foil $[-1/0\ 1/3\ 0/1]_i$ (the $A2P_1$ axis) upon annealing at 550°C for 4 and 8 h; (b) lamellae of the $P1$-, $P2$-, and $i$-phases for the orientation of the foil $[0/0\ 0/2\ 0/0]_i$ (the $A2_3$ axis) upon annealing at 550°C for 10 and 24 h; and (c) polygrain $i$-phase upon annealing at 650°C for 8 h. In all cases, the operating reflections are of the types $(2/3\ 0/0\ 1/2)_i$ and $(2/3\ 0/0\ -1/\ -2)_i$.

periodic law, the system of new reflections is observed in the electron diffraction patterns obtained in the direction of the twofold symmetry axis $A2$ (Fig. 1) and the mirror plane axis $A2P$ nearest to it. These reflections are arranged periodically along the fivefold symmetry axis, which is perpendicular to the plane of defects, and aperiodically in the plane of defects. The analysis of the experimental electron diffraction pattern and the pattern calculated for the perfect icosahedral structure as well as the determination of the components of the displacement vector **R** at the boundary of defects were carried out in our previous work [14]. It was shown that planar defects are intergrowths of the $P1$-pentagonal approximant, and the formation of the lattice of the $P1$-approximant occurs in accordance with the phason mechanism and is determined by the matrix of the phason displacement [12, 13]. The positions of the reflections of the $P1$-phase, determined from the experiment, are in close agreement with those calculated using the matrix of the phason displacement $i \longrightarrow P1$.

The formation of interlayers of the $P1$-phase in the icosahedral matrix has been considered by us as a result of the nonequilibrium transformation $i$-quasicrystal $\longrightarrow$ pentagonal phase, which is initiated both by local deviations of the chemical composition and by the strain state that is typical of rapidly quenched alloys [14]. It can be assumed that an increase in the annealing time will lead to a further development of the transformation as well as to the formation of interlayers of the $P2$-pentagonal approximant, which is characteristic of transformations of the $i$-phase in rapidly quenched alloys with compositions in the region of its structural instability [12, 20]. This process can be accompanied by the formation of a homogeneous lamellar structure with alternating interlayers of the $P1$- and $P2$-phases.

Extended regions with the lamellar structure are observed already in the two-phase ($i + P1$) state. The quasicrystal-forming $Al_{62.2}Cu_{24.8}Fe_{13}$ and $Al_{61.7}Cu_{25.2}Fe_{13.1}$ alloys annealed for 10 or 24 h are characterized by the formation of a homogeneous lamellar structure with the boundaries aligned parallel to the planes with the fivefold symmetry axes $A5$ (Fig. 2b). A comparison between the experimental electron diffraction patterns obtained in the direction of the twofold symmetry axis $A2$ and the corresponding diffraction pattern calculated for the perfect quasicrystalline structure has revealed the presence of additional diffraction spots and diffuse effects (Figs. 3c, 3d).

Additional diffraction effects observed for the alloy subjected to long annealings can be attributed to two additional reciprocal lattices. The translation vectors of the reciprocal lattice $|\mathbf{g}_{period}|$, which are associated with the physical reciprocal space, have the following relationships with the reciprocal lattice vector for the reflection $(2/3\ 0/0\ -1/\ -2)$ of the $i$-phase: $|\mathbf{g}_{period}| = 1/25|\mathbf{g}_{||}(2/3\ 0/0\ -1/\ -2)| = 1/52.3\ Å^{-1}$ for the first lat-

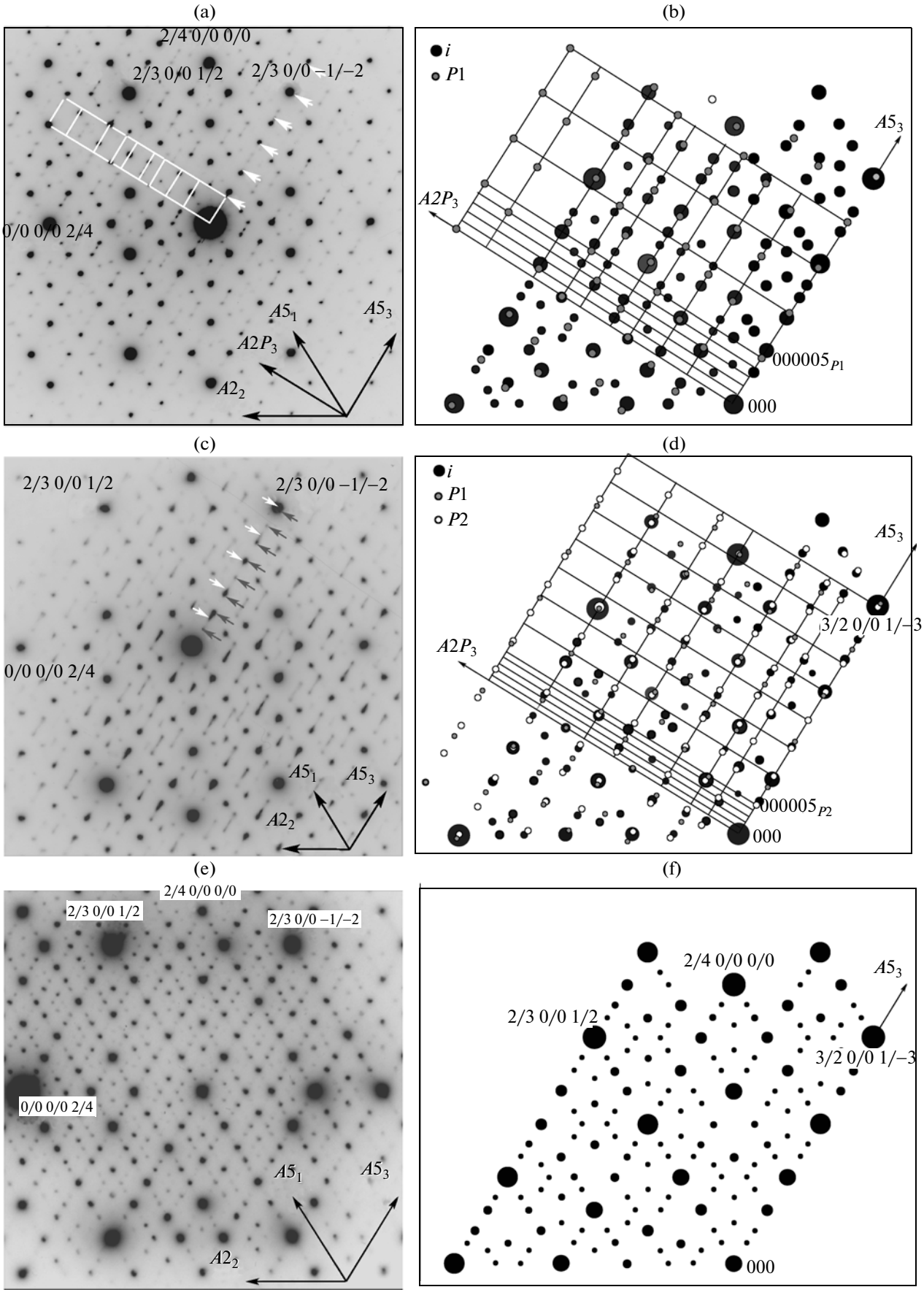
(a)
2/4 0/0 0/0
2/3 0/0 1/2
2/3 0/0 –1/–2
0/0 0/0 2/4
$A5_1$
$A5_3$
$A2P_3$
$A2_2$
(b)
i
P1
$A5_3$
$A2P_3$
$000005_{P1}$
000
(c)
2/3 0/0 1/2
2/3 0/0 –1/–2
0/0 0/0 2/4
$A5_1$
$A5_3$
$A2_2$
(d)
i
P1
P2
$A5_3$
3/2 0/0 1/–3
$A2P_3$
$000005_{P2}$
000
(e)
2/4 0/0 0/0
2/3 0/0 1/2
2/3 0/0 –1/–2
0/0 0/0 2/4
$A5_1$
$A5_3$
$A2_2$
(f)
2/4 0/0 0/0
$A5_3$
2/3 0/0 1/2
3/2 0/0 1/–3
000

**Fig. 3.** (a, c, e) Electron diffraction patterns obtained for the annealed alloys $Al_{62.2}Cu_{24.8}Fe_{13}$ and $Al_{61.7}Cu_{25.2}Fe_{13.1}$ and (b, d, f) corresponding calculated schemes: (a, b) alloys with interlayers of the *P*1-phase in the *i*-matrix; (c, d) alloys with the lamellar structure of the *P*1-, *P*2-, and *i*-phases; and (e, f) alloys with the single-phase polygrain *i*-structure for the orientation of the foil in the [0/0 0/2 0/0] direction (the $A2_3$ axis). Bright and dark arrows indicate the positions of periodic reflections of the *P*1- and *P*2-pentagonal phases in the zeroth row.

tice and $|\mathbf{g}_{\text{period}}| = 1/40|\mathbf{g}_{\|}(2/3\ 0/0\ -1/-2)| = 1/83.9$ Å$^{-1}$ for the second lattice. These translation vectors correspond to periodicities of the reciprocal lattices of the two *P*1- and *P*2-pentagonal phases, whereas only the *P*1-phase is observed in the alloys annealed for 4 and 8 h (Figs. 3a, 3b). The positions of reflections of both sublattices on the experimental electron diffraction patterns coincide with the positions of reflections of the *P*1- and *P*2-phases, which were calculated using the matrix $\varepsilon_{i\to P}$ of the linear phason displacement proposed in [12]:

$$[\mathbf{g}_{\|P}] = [\mathbf{g}_{\|t}] + {}^{t}\varepsilon_{t\to P}[\mathbf{g}_{\perp t}], \tag{6}$$

$$ {}^{t}\varepsilon_{t\to P1} = \frac{1}{\tau^{4}\tau^{1/2}}\begin{pmatrix} 1 & (-\tau)^{-1} & 0 \\ \tau & -1 & 0 \\ 0 & 0 & 0 \end{pmatrix}, $$

$$ {}^{t}\varepsilon_{t\to P2} = \frac{-1}{\tau^{6}\times 5^{1/2}}\begin{pmatrix} 1 & (-\tau)^{-1} & 0 \\ \tau & -1 & 0 \\ 0 & 0 & 0 \end{pmatrix}, \tag{7}$$

where $[\mathbf{g}_{\|P1}]$ and $[\mathbf{g}_{\|P2}]$ are the reciprocal lattice vectors of the *P*1- and *P*2-pentagonal approximants in the physical space.

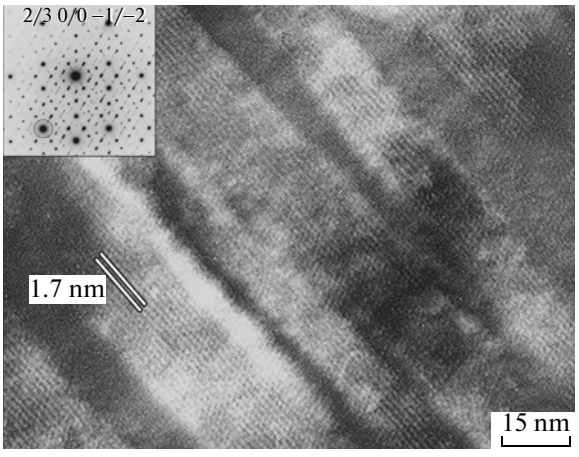


**Fig. 4.** Image of the (000005) periodic lattice planes of the *P*2-pentagonal phase with $\Delta d$ = 1.69 nm in individual lamellae of the $Al_{62.2}Cu_{24.8}Fe_{13}$ alloy ($T_{\text{ann}}$ = 550°C, 24 h) for the orientation of the foil [0/0 0/2 0/0] parallel to the $(000001)_{P2}$ planes. The inset shows the operating reflections in the diffraction pattern.

We obtained the images of the lattice in two reflections of the *P*2-phase with $\Delta d = d_{000005} = 16.9$ Å for the strict orientation of the foil in the direction of the twofold symmetry axis *A*2 (Fig. 4, inset). The images obtained for the Al–Cu–Fe alloys annealed for 24 h indicate that only single lamellae belong to the *P*2-phase. The other lamellae, apparently, have the structure of the *i*-phase and *P*1-pentagonal approximant.

The stable single-phase polygrain icosahedral structure of the $Al_{62.2}Cu_{24.8}Fe_{13}$ and $Al_{61.7}Cu_{25.2}Fe_{13.1}$ alloys is formed as a result of the annealing of the rapidly quenched state at a temperature of 650°C for 8 h (Fig. 2c). In the electron diffraction patterns, there are only diffraction spots in the positions corresponding to the calculated bcc reciprocal lattice of the perfect icosahedral structure of the Al–Cu–Fe system (Figs. 3e, 3f).

The electron microscopy and electron diffraction investigations of the kinetics of structural phase transformations have demonstrated that an increase in the time of annealing at a temperature of 550°C in the quenched quasicrystal-forming $Al_{62.2}Cu_{24.8}Fe_{13}$ and $Al_{61.7}Cu_{25.2}Fe_{13.1}$ alloys with compositions in the region of stability of the *i*-phase results in the development of the successive nonequilibrium phase transformations $i \longrightarrow P1$ and $i \longrightarrow P2$. The three-phase ($i$ + *P*1 + *P*2) state leads to the formation of a homogeneous lamellar structure of the alloy with sizes of lamellae ranging from 200 to 400 Å.

The next subsection presents the results of nanoindentation tests for two types of quasicrystalline alloys: (i) alloys with the lamellar structure of pentagonal phases and (ii) alloys with the single-phase polygrain icosahedral structure.

### *3.2. The P–h Diagrams and Nanomechanical Characteristics of Quasicrystalline Al–Cu–Fe Alloys with the Lamellar and Polygrain Structures, Hardening Effects*

Typical *P*–*h* loading diagrams obtained for the quasicrystalline $Al_{62.2}Cu_{24.8}Fe_{13}$ alloys with the polygrain icosahedral and lamellar structures are shown in Fig. 5. Similar loading diagrams were obtained for the $Al_{61.7}Cu_{25.2}Fe_{13.1}$ alloy. In all the loading diagrams, there are nonlinear parts of the loading branches, and the residual indentations have large depths ($h_f \sim (0.6–0.7)h_{\max}$). This corresponds to the plastic deformation mode, which was previously

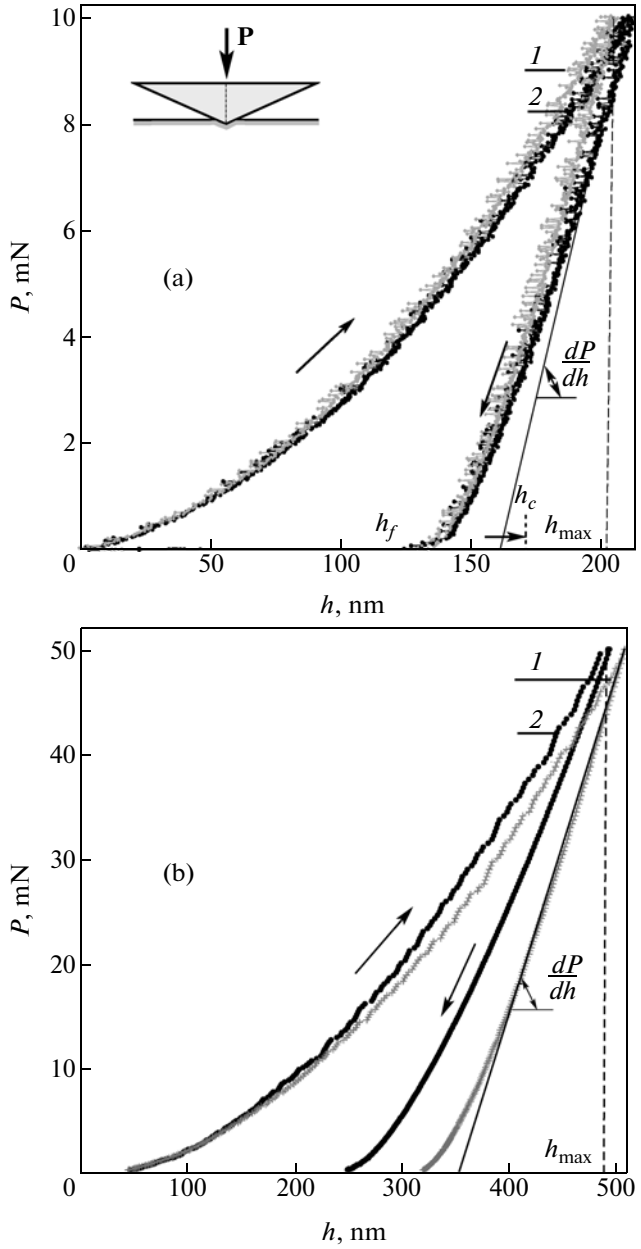


**Fig. 5.** *P*–*h* loading diagrams of the quasicrystal-forming $Al_{62.2}Cu_{24.8}Fe_{13}$ alloys with (*1*) polygrain icosahedral structure and (*2*) lamellar structure. $P_{max}$ = (a) 10 and (b) 50 mN.

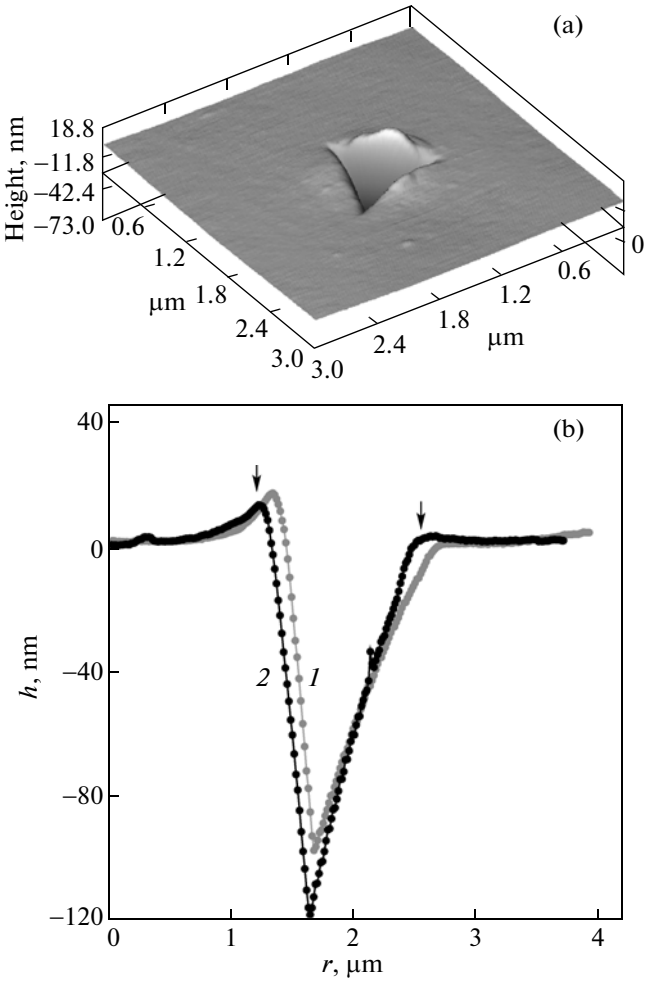


**Fig. 6.** (a) AFM-image and (b) scanned profiles of indentations after unloading for the quasicrystalline Al–Cu–Fe alloys at $P_{max}$ = 10 mN: (*1*) alloy with the polygrain icosahedral structure and (*2*) alloy with the lamellar structure. Arrows indicate pile-ups.

observed during nanoindentation of quasicrystalline alloys with icosahedral and decagonal structures [6–10].

The contribution from the plastic deformation was also determined from the atomic force microscopy (AFM) data. The AFM images and scanned profiles of the indentations (Fig. 6) demonstrate pile-ups that are typical of plastically deformed materials [21], including quasicrystals [22]. The scanning electron microscopy (SEM) images of the indentations obtained at the maximum loads $P_{max}$ = 50 and 500 mN also demonstrate pile-up effects at the indentation edges with a bleached contrast (Fig. 7). In all the loading curves, there are signs of unstable plastic deformation (jumps and steps), which is characteristic of quasicrystalline structures [8, 9]. These effects are most pronounced in the loading curves obtained at maximum loads $P_{max} \geq$ 50 mN.

Thus, both types of quasicrystal-forming alloys exhibit similar qualitative features of elasto-plastic deformation, which are typical of quasicrystals during nanoindentation. At the same time, the analysis of the quantitative loading parameters and calculated mechanical characteristics has revealed significant differences in the behavior of the alloys with polygrain icosahedral and lamellar structures (Tables 1, 2, Fig. 8).

The dependences of the contact hardness *H* on the applied maximum load $P_{max}$ for both types of alloys are shown in Fig. 8. It can be seen from this figure that, for

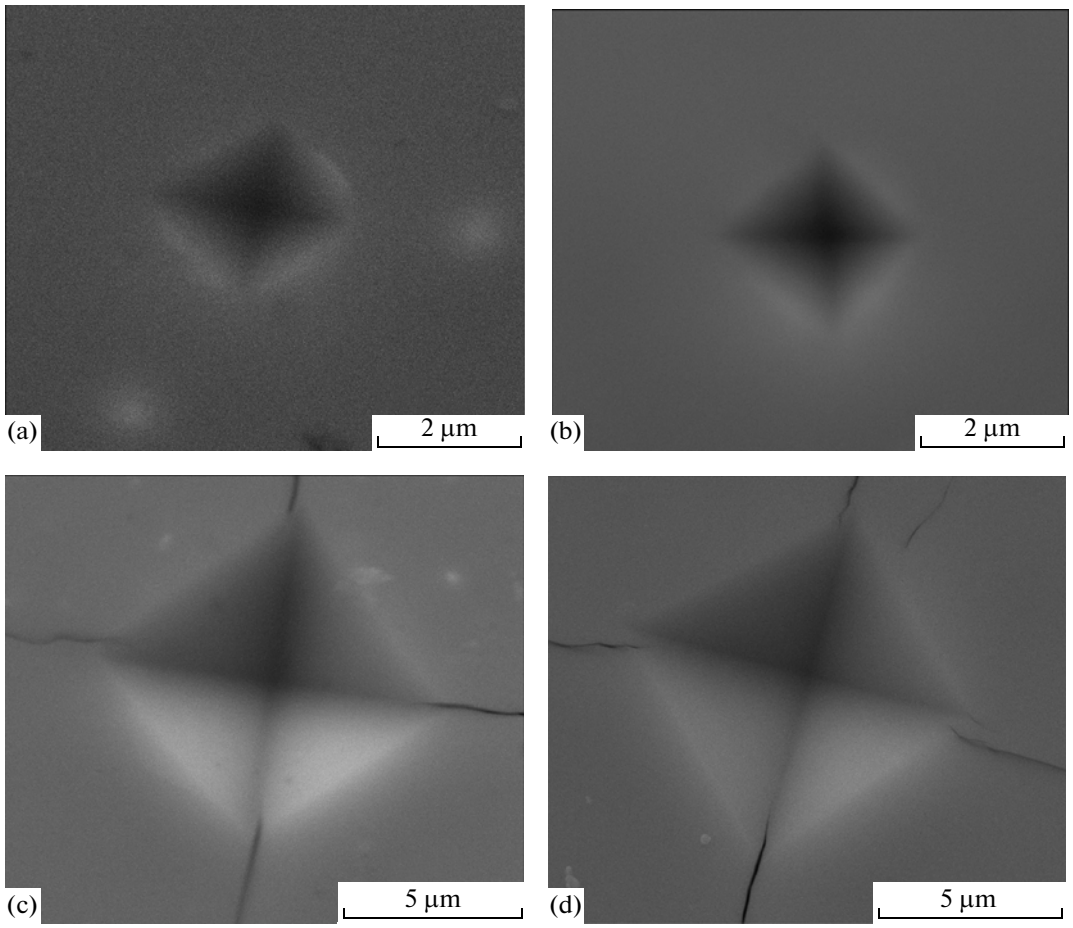


**Fig. 7.** SEM images of residual indentations for quasicrystalline alloys with (a, c) lamellar structure of the pentagonal phases and (b, d) polygrain icosahedral structure at the maximum loads $P_{max}$ = (a, b) 50 and (c, d) 500 mN.

the alloys with the polygrain icosahedral structure in the range of loads up to 50 mN, the hardness remains unchanged within the limits of the measurement error, whereas over the entire range of loads from 5 to 500 mN, the hardness on the whole decreases in accordance with the normal size effect that is characteristic of quasicrystalline alloys [9, 23]. The Meyer law [24], which accounts for the normal size effect,

$$P_{max} = Ch_c^n \quad (8)$$

(where $C$ is an empirical constant), with good accuracy describes the relationship between the maximum load and the contact depth for the alloys with the polygrain icosahedral structure (Fig. 9). In this relationship, the exponent has the value $n = 1.846$. The samples with the polygrain icosahedral structure already in the range of loads $P_{max} \geq 100$ mN have the hardness of ~10 GPa (Table 1), which is close to the values available in the literature for quasicrystalline Al–Cu–Fe alloys at high loads [4]. The value of the exponent $n$ of less than 2 in the Meyer relationship means that hardening effects are not observed for polygrain icosahedral quasicrystalline alloys [24, 25].

The dependences of the hardness on the maximum load for the alloys with the lamellar structure, in contrast to the samples with the polygrain icosahedral structure, always have a pronounced nonmonotonic character with a maximum (Fig. 8). From the point of view of the indentation size effects, a similar type of

**Table 1.** Parameters of the $P$–$h$ loading diagrams and mechanical characteristics for the quasicrystalline alloy with the polygrain icosahedral structure

| Parameter/characteristic | $P$, mN | | | | |
|---|---|---|---|---|---|
| | 5 | 10 | 50 | 100 | 500 |
| $h_{max}$, nm | 136 | 202 | 512 | 754 | 1819 |
| $h_c$, nm | 107 | 162 | 404 | 606 | 1441 |
| $A$, μm$^2$ | 0.410 | 0.827 | 4.0 | 8.8 | 49.6 |
| $H$, GPa | 12.2 | 12.1 | 12.3 | 11.3 | 10.0 |

Note: The error determined from the spread of measurements is less than 5%.

**Table 2.** Parameters of the $P$–$h$ loading diagrams and mechanical characteristics for the quasicrystalline alloy with the lamellar structure of the $P1$- and $P2$-pentagonal approximants

| Parameter/characteristic | $P$, mN | | | | |
|---|---|---|---|---|---|
| | 5 | 10 | 50 | 100 | 500 |
| $h_{max}$, nm | 136 | 204 | 498 | 750 | 2004 |
| $h_c$, nm | 106 | 163 | 373 | 566 | 1462 |
| $A$, μm$^2$ | 0.41 | 0.83 | 3.3 | 7.6 | 50.1 |
| $H$, GPa | 12.2 | 12.1 | 15.1 | 13.1 | 10.0 |

Note: The error determined from the spread of measurements is less than 5%.

**Table 3.** Meyer hardness $H$ and plastic hardness $H_{PI}$ for quasicrystalline alloys with the polygrain icosahedral and lamellar structures

| Parameter | $i$-phase (polygrain structure) | | | $i$-phase + $P$-phases (lamellar structure) | | |
|---|---|---|---|---|---|---|
| | $P_{max}$, mN | | | $P_{max}$, mN | | |
| | 50 | 100 | 500 | 50 | 100 | 500 |
| $H$, GPa | 12.3 | 11.3 | 10 | 15.1 | 13.1 | 10 |
| $H_{P1}$, GPa | 14.5 | 12.6 | 11.3 | 18.2 | 15.7 | 12.1 |

dependences of the hardness $H$ on the maximum load $P_{max}$ is considered as a transition from the normal to reverse size effect. In the case where crack formation does not occur, the mechanism of this transition is determined by specific features in the development of plastic deformation [25, 26], for example, by the replacement of slip planes with different activation energies in the case of single crystals or by the effects of strain hardening and further softening. The formation of cracks in the alloys studied in this work begins to occur at maximum loads of greater than 100 mN. The observed peak character of the dependence of the hardness on the load and, on the whole, the increase in the hardness at loads of 50 mN should be considered as the hardening effect in the alloys with the lamellar structure. This is consistent with the higher values of the plastic hardness $H_{PI}$ (Table 3) in the range of loads $P_{max} \geq 50$ mN for the alloys with the lamellar structure as compared to the polygrain icosahedral quasicrystalline alloys.

The mechanism of the revealed hardening effect in the alloys with the lamellar structure, in our opinion, is associated not with the mechanical properties of the pentagonal approximant phases, but with the difficulties in the development of plastic deformation at the boundaries of lamellae. During nanoindentation, the approximant phases with a two-dimensional aperiodicity will behave like two-dimensional decagonal quasicrystalline phases, which, as is known, exhibit the normal size effect and have lower values of the contact hardness than the three-dimensional quasicrystals [23].

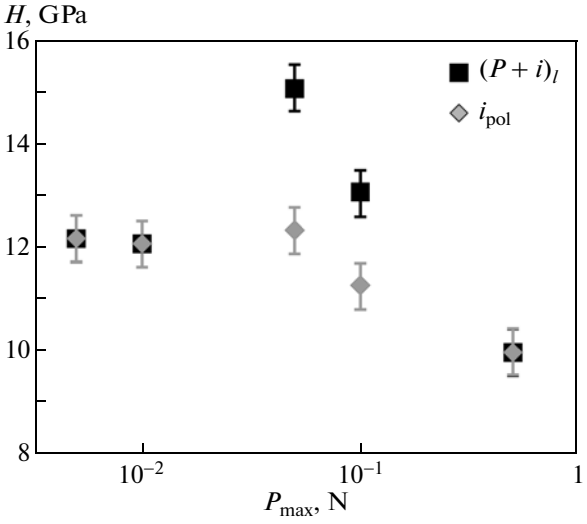


**Fig. 8.** Dependences of the hardness $H$ on the maximum load $P_{max}$ for the quasicrystalline alloys $Al_{61.7}Cu_{25.2}Fe_{13.1}$ and $Al_{62.2}Cu_{24.8}Fe_{13}$ with the polygrain icosahedral structure ($i_{pol}$) and lamellar structure of the pentagonal phases $(P+i)_l$ in the load range 5 mN $\leq P_{max} \leq$ 500 mN.

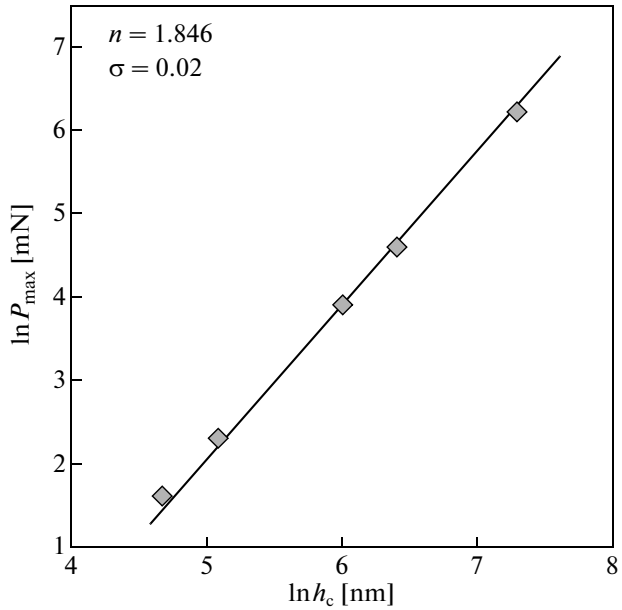


**Fig. 9.** Dependence of $\ln P_{max}$ on $\ln h_c$ according to the Meyer relationship for the quasicrystalline Al–Cu–Fe alloy with the polygrain icosahedral structure.

## 4. CONCLUSIONS

The kinetics of transformations during annealing of the quenched quasicrystal-forming alloys $Al_{62.2}Cu_{24.8}Fe_{13}$ and $Al_{61.7}Cu_{25.2}Fe_{13.1}$ with compositions in the region of stability of the icosahedral ($i$) phase has been investigated using transmission electron microscopy and electron diffraction with the projection and cut method in the six-dimensional space. It has been found that an increase in the annealing time at a temperature of 550°C leads to the development of successive nonequilibrium transformations $i \longrightarrow P1$ and $i \longrightarrow P2$. In the three-phase ($i + P1 + P2$) state, a homogeneous lamellar structure with sizes of lamellae ranging from 200 to 400 Å is formed, thus replacing single nanoscale interlayers of the $P1$-phase in the icosahedral matrix in the two-phase ($i + P1$) state. The single-phase icosahedral structure is formed as a result of annealing at 650°C.

The $P$–$h$ loading diagrams, as well as the AFM and SEM data, have demonstrated that both types of quasicrystalline alloys (with polygrain icosahedral and lamellar structures) in the range of loads 5 mN $\le P_{max} \le$ 500 mN show signs of elasto-plastic deformation.

For the alloys with the polygrain icosahedral structure, the dependence of the contact hardness $H$ on the maximum load $P_{max}$ has a normal size effect. The alloys with the lamellar structure in the range of loads 50 mN $\le P_{max} <$ 500 mN are characterized by a higher hardness $H$ and an increase in the plastic hardness $H_{Pl}$ as compared to the polygrain icosahedral alloys and exhibit the effect of strain hardening in the dependence of the hardness $H$ on the maximum load $P_{max}$. The strain hardening is considered as the result of resistance exerted by the boundaries of the nanoscale lamellar structure to plastic deformation.

## ACKNOWLEDGMENTS

We would like to thank A.N. Uksusnikov and E.N. Frizen for their technical assistance in performing the experiments.

This study was supported by the Russian Foundation for Basic Research (project no. 10-02-00602a).

The electron microscopy investigations were carried out at the Center for Collective Use "Electron Microscopy" (Ural Branch of the Russian Academy of Sciences, Yekaterinburg, Russia).

## REFERENCES

1. M. Feuerbacher and K. Urban, in *Quasicrystals, Structure and Physical Properties*, Ed. by H. R. Trebin (Wiley, Weinheim, 2003), p. 431.
2. K. Urban, M. Feuerbacher, M. Wollgarten, and M. Bartsch, in *Physical Properties of Quasicrystals*, Ed. by Z. Stadnik (Springer-Verlag, Berlin, 1999), p. 365.
3. K. Tanaka, Y. Mitara, and M. Koiwa, Philos. Mag. **73**, 1715 (1996).
4. E. Giacometti, N. Baluc, J. Bonnevile, and J. Rabier, Scr. Mater. **41**, 989 (1999).
5. F. Fleury, S. M. Lee, W. T. Kim, and D. H. Kim, Metall. Mater. Int. **6**, 415 (2000).
6. J. M. Dubois, *Useful Quasicrystals* (World Scientific, Singapore, 2005), p. 462.
7. J. Von Steubut, C. Strobel, and J. M. Dubois, in *Proceedings of the 5th International Conference on Quasicrystals, Avignon, France, May 22–26, 1995*, Ed. by C. Jano and R. Mosseri (World Scientific, Singapore, 1995), p. 704.
8. S. N. Dub, Yu. V. Milman, D. V. Lotsko, and A. N. Belous, J. Mater. Sci. Lett. **20**, 1043 (2001).
9. P. Paufler and B. Wolf, in *Quasicrystals, Structure and Physical Properties*, Ed. by H. R. Trebin (Wiley, Weinheim, 2003), p. 431.
10. Yu. I. Golovin, S. N. Dub, V. I. Ivolgin, V. V. Korenkov, and A. I. Tyurin, Izv. Akad. Nauk, Ser. Fiz. **68**, 1428 (2004).
11. Yu. V. Milman, D. V. Lotsko, S. N. Dub, A. I. Ustinov, S. S. Poloshcuk, and S. V. Ulshin, Surf. Coat. Technol. **201** (12), 5937 (2007).
12. N. Menguy, M. Audier, P. Guyot, and M. Vacher, Philos. Mag. B **68** (5), 595 (1993).
13. M. Quiquandon, A. Quivy, J. Devaud, F. Faudot, S. Lefebvre, M. Bessière, and Y. Calvayrac, J. Phys.: Condens. Matter **8** (15), 2487 (1996).
14. E. V. Shalaeva, A. F. Prekul, S. Z. Nazarova, and V. V. Khiller, Phys. Solid State **54** (4), 699 (2012).
15. W. C. Oliver and G. M. Pharr, J. Mater. Res. **7**, 1564 (1992).
16. S. I. Bulychev, V. P. Alekhin, M. Kh. Shorshov, A. P. Ternovskii, and G. D. Shnyrev, Zavod. Lab. **41**, 1137 (1975).
17. J. W. Cahn, D. Shechtman, and D. Gratias, J. Mater. Res. **1**, 13 (1986).
18. C. Jano, *Quasicrystals* (Clarendon, Oxford, 1994), p. 423.
19. J. D. Rzepski, A. Quivy, Y. Calvayrac, M. C. Quiquandon, and D. Gratias, Philos. Mag. B **60**, 855 (1989).
20. D. Gratias, Y. Calvarayc, J. Devaud-Rzepski, F. Faudot, M. Harmelin, A. Quivy, and P. A. Bancek, J. Non-Cryst. Solids **135–154**, 482 (1993).
21. A. Bolshakov and G. M. Pharr, J. Mater. Res. **13**, 1049 (1998).
22. X. Li, L. Zhang, and H. Gao, J. Phys. D: Appl. Phys. **37**, 745 (2004).
23. N. K. Mikhopadhyay, G. C. Weatherly, and J. D. Embry, Mater. Sci. Eng., A **315**, 202 (2001).
24. E. Meyer, VDI Z. (1857–1968) **52**, 645 (1908).
25. B.Wolf, S. Swain, M. Kempf, and P. Paufler, J. Mater. Sci. **35**, 723 (2000).
26. K. Sangwall, Mater. Chem. Phys. **63**, 145 (2000).

*Translated by O. Borovik-Romanova*